



CHALMERS
UNIVERSITY OF TECHNOLOGY



Vortex

Designing a fountain with CFD analysis

Master's thesis in Innovative and Sustainable Chemical Engineering

KRISTIAN MÅLBAKKEN

MASTER'S THESIS 2015:09

Vortex

Designing a Fountain With CFD

KRISTIAN MÅLBAKKEN



CHALMERS
UNIVERSITY OF TECHNOLOGY

Department of Chemistry and Chemical Engineering
CHALMERS UNIVERSITY OF TECHNOLOGY
Gothenburg, Sweden 2015

Vortex
Designing a Fountain With CFD
KRISTIAN MÅLBAKKEN

© KRISTIAN MÅLBAKKEN, 2015.

Supervisor/Examiner:
Ronnie Andersson, Department of Chemistry and Chemical Engineering

Master's Thesis 2015:09
Department of Chemistry and Chemical Engineering
Chalmers University of Technology
SE-412 96 Gothenburg
Telephone +46 31 772 1000

Cover: Photo of the fountain in action with added lighting.
Typeset in L^AT_EX
Printed by [Name of printing company]
Gothenburg, Sweden 2015

Vortex

Designing a fountain with CFD analysis

KRISTIAN MÅLBAKKEN

Department of Chemistry and Chemical Engineering

Chalmers University of Technology

Abstract

This thesis has been part of the Physics and Arts forum at the faculty of Physics at Chalmers University of Technology. The work presented in this thesis is about understanding the physics of the artwork Vortex and use the results as guidelines for improving it in terms of stability. To gain an insight to the physics of the fountain, both experiments and simulations using computational fluid dynamics has been used. This thesis will try to build a better understanding of the fountain utilizing a transition sensitive model in order to be able to select between different designs. Seeing that the physics in this fountain is extremely complex, some simplifications has to be made, this will mean solving for a 2D axisymmetric problem. With hands on experience and calculations, a baffle was introduced to dampen the waves seen in the reservoir. Later a turbulence dampener in the form of an aquarium filter was fitted to minimize the turbulent kinetic energy in the flow prior to free fall. To further reduce the energy in the flow, the edge from the water reservoir to the ledge was smoothed out. Experiments show that the falling film drastically improves when these measures are taken. It is observed that without these measures, the flow on the ledge is turbulent at all times, the flow is only intermittently turbulent when modifications are in place. Also a significantly better trajectory can be observed at the higher flow rates. Results from the CFD analysis shows that the less profound edge from water reservoir to the ledge completely eliminates the separation of the flow and swirling at the edge, making it less likely to transition to turbulent flow. The filter placed before this ledge can also be shown to eliminate a great deal of the turbulence that enters the ledge, thus minimizing the fluctuation energy that might contribute to a transition ergo making the fountain more stable.

Keywords: ANSYS, CFD, Fountain, Art, Water curtain, Water film, Multiphase.

Acknowledgements

I would like to thank my supervisor associate professor Ronnie Andersson for helping and pointing me in the right direction in moments of despair .I also want to thank my supervisor Dr. Ruben Avila on site at UNAM, Mexico City, Mexico for helping me attack the problem at hand in a different perspective. I would like to thank the Souza family and friends for an amazing time in Mexico. I came to Mexico alone, but left with a family. Last, but not least I would like to thank my parents for always supporting me. Also, I would like to high five my self for finishing this thesis.

Kristian Målbakken, Gothenburg, July 2015

Contents

1	Introduction	1
1.1	Objective	3
1.2	Scope of Work	3
2	Theory	5
2.1	Laminar-Turbulent Transition	5
2.2	Governing Equations	7
2.2.1	Non-Dimensional Analysis	8
2.3	Analytical Solution	9
2.4	Modelling	10
2.4.1	Turbulence	10
2.4.2	k - kl - ω - Turbulence Model	11
2.4.3	Volume of Fluid	12
2.5	Fluttering	13
3	Experimental Set-up and Methods	15
3.1	Geometry	15
3.2	Experiments	17
3.2.1	Trajectory and Fluttering	17
3.2.2	Turbulence	18
3.3	Simulations	18
3.3.1	Mesh	18
3.3.1.1	Adapting Mesh	19
3.3.2	Pressure Drop	20
3.3.3	Numerical methods	21
4	Results and Discussions	23
4.1	Full Scale Experiments and Simulations	23
4.1.1	Trajectory	23
4.1.2	Fluttering	24
4.2	Turbulence	24
4.3	Velocities at Ledge	26
4.4	Edge effects	27
4.5	Discussion	30
5	Conclusion	31
5.1	Future studies	32

Bibliography

32

1

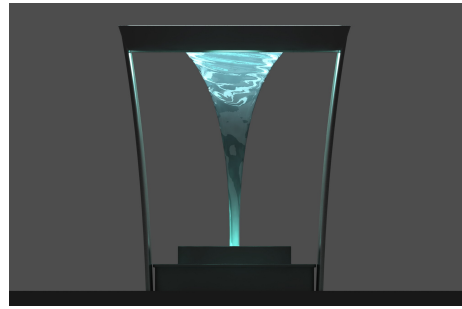
Introduction

Pål Svensson is one of the most renowned sculptural artist in Sweden. He has completed more than 30 public artworks, won several competitions and had more than 20 separate vernissages. His main source of inspiration is nature and most of his artworks are made in stone. The sculpture/fountain Vortex takes inspiration in nature from the swirling motion of water and how it can be dramatised, hence the name of the artwork. The project is part of Chalmers University of Technology's physics and art forum which aims to combine engineering and art. The idea for the design where conceived during 2006 during an exhibition by the artist himself, held in Chelsea, New York. A number of possible designs where shortly after visualised by Daniel Hultman (White arkitekter). Some of the concepts are shown on the following page. The work on the fountain began after some simple Lagrangian models where made for the water trajectory, and a first prototype was made. The work of this thesis would help shape the future design of the artwork with the results obtained. There exists so called "inverted fountains", and waterfall fountains that consists of a laminar sheet of water falling under the influence of gravity [1], but there are none that consists of a circular waterfall. Annular free-falling sheets of water has been well studied [1], and are created when placing a disc obstruction in front of a water jet. These studies concludes that the height of the water bell has a certain hight after which it becomes unstable or contracts due to pressure difference. This artwork will be unique with its inverted design, where water flows from the top creating a circular waterfall and later converge in in a single point.

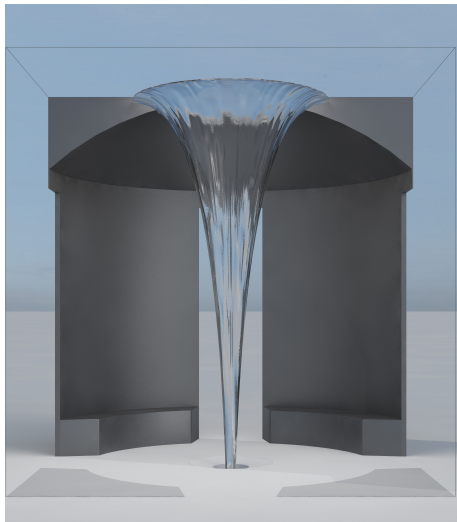
The aim of this thesis is to gain a deeper understanding of the water flow and the underlying physics. This thesis will investigate the effect of different ledge design, reservoir design and different operating conditions. The goal is to be able to use the results to make the fountain as stable as possible and as unaffected by disturbances as possible. To gain a deeper understanding of how the water flow in the fountain works, computational fluid dynamics (CFD) will be used to understand different designs and different flow rates.



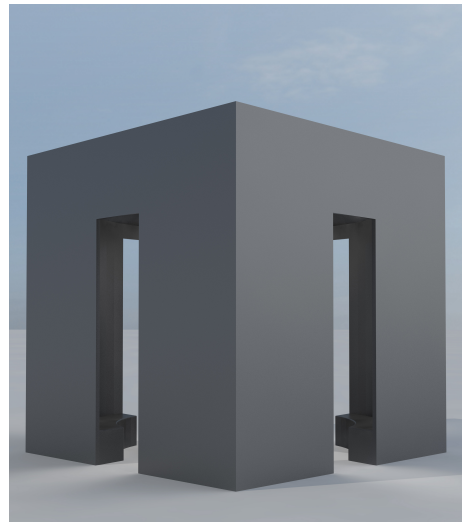
(a) Concept 1 in urban environment.



(b) Sideview of concept 1.



(c) Concept 2 cut in half, displaying the inside.



(d) Isoview of concept 2.

Figure 1.1: Concepts for the design of the fountain.

1.1 Objective

The main objective of this thesis is to gain a better understanding of the water flow in the fountain to be able to improve the stability, which is believed to be affected by disturbances of the water feed to the reservoir and turbulence on the water film on the inclined ledge. This will be done studying the effect of several design and operating parameters using CFD supported by experiments.

1.2 Scope of Work

- Gain a better understanding of the physics of the fountain, mainly in the water reservoir.
- Analyse the effects of the turbulence filter.
- Study the effects of adding baffles in the water reservoir.
- Analyse the effects of a less pronounced edge from water reservoir to ledge.
- Understand the numerics; dynamic grid adaptation, multiphase flow, transition turbulence modelling.
- Give design recommendations based on the results.

Demarcations.

Due to lack of time and resources the problem will be solved as a 2D axisymmetric problem. Given the complexity of the problem, the focus of this thesis will be on the physics in the water reservoir and geometry before free fall. Alterations of any kind of the properties, such as viscosity, were not investigated as the artist requested pure water to be used. External forces and disturbances, such as wind, will not be investigated.

2

Theory

The following chapter will introduce a brief background to the physical phenomena and the theory used in this thesis. Much attention will be focused on explaining and understanding the physics of laminar to turbulent transition as it plays a key-role in how the fountain operates and its stability. Governing equations, theory for the numerics and turbulence models as well as multiphase theory will also be introduced in the following chapter.

2.1 Laminar-Turbulent Transition

The field of laminar to turbulent transition has been of great academic interest for more than a century [2], and it has been concluded that the transition from laminar to turbulent flows have a great impact on the characteristics of the flow in applications such as marine propellers [3], turbo machinery [2] [4], flow in airways [5] and in other applications. However, transition from laminar to turbulent flow is not yet fully understood [4, 6], but some consensus about the main factors leading to transition has been reached [7]. There are two main pathways from laminar to turbulent flow, namely natural- and bypass transition. The disturbance and transition from laminar to turbulence on a flat plate happens in three stages [2].

The main phenomena that leads to instability in the laminar boundary layer, given that the free stream turbulence is low $\leq 1\%$, are the two-dimensional Tollmien-Schlichting waves [8]. These waves were first discovered by solving the Orr-Sommerfeld equation [7] and later proved to exist in experiments [9]. These waves are of low frequency and will either decay or amplify (spatially or temporally). This is the first step in natural transition. Downstream of the first observed Tollmien-Schlichting waves, *intermittent* turbulent spots appears. The inside of these intermittent spots are fully turbulent, and the spots themselves are observed to be moving with characteristic velocities [10]. The described pathway from laminar to turbulent flow by Tollmien-Schlichting waves are known as *natural transition*. It is worth noting that the experiments confirming this have been done with extremely low free-stream turbulence intensity ($\leq 0.1\%$).

Another pathway to turbulence is the *bypass transition* route. Bypass in this sense means it bypasses the natural transition. This mechanism relies on higher free stream turbulence than 1% , which is often the case in turbo machinery and in aeronautics [11–13]. These instabilities are thought to arise when the boundary layer acts as a high-pass filter where the high frequency components from the free stream turbulence are amplified and the low frequency components are damped [14, 15].

The streamwise perturbations are known as Klebanoff modes [16, 17].

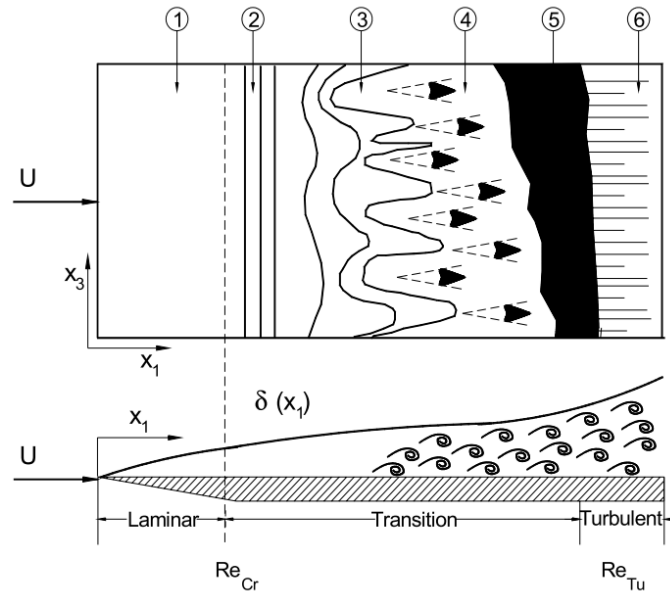


Figure 2.1: Sketch of transition process in the boundary layer along a flat plate at zero pressure gradient, a composite picture of features in [18] after White [19]. Figure and caption from Schobeiri [2].

1. A stable laminar flow is established that starts from the leading edge and extends to the point of inception of the unstable two-dimensional Tollmien-Schlichting waves.
2. Onset of the unstable two-dimensional Tollmien-Schlichting waves.
3. Development of unstable, three-dimensional waves and the formation of vortex cascades.
4. Bursts of turbulence in places with high vorticity.
5. Intermittent formation of turbulent spots with high vortical core at intense fluctuation.
6. Coalescence of turbulent spots into a fully developed turbulent boundary layer.

The transition from laminar to turbulent will not go from fully laminar to fully turbulent spontaneously at one point in space, it will gradually turn more and more chaotic as explained in Figure 2.1. A concept that is widely adopted is the use of the term *intermittency*, which is a measurement of how long the flow is fully turbulent at one point of space. Early research described the flow as intermittently turbulent for a while before transitioning to fully turbulent. In Figure 2.1, it is shown that at point 5 there is a formulation of turbulent spots, earlier research referred to these spots as "islands" or wedges [18]. These turbulent islands would form triangles as an effect of the different velocities at different locations [18]. The fraction of the total time a flow at a certain point is turbulent can be quantified and expressed as what can be called an *intermittency factor*. The intermittency factor γ can be expressed as [2]:

$$\gamma(x) = \frac{1}{N} \sum_{i=1}^N I(x, t_i) \quad (2.1)$$

where $I(x, t)$ is the intermittency function. The intermittency function is defined as following:

$$I(x, t) = \begin{cases} 1 & \text{for turbulent flow} \\ 0 & \text{for non-turbulent flow} \end{cases} \quad (2.2)$$

2.2 Governing Equations

This problem is highly complex and needs to be simplified to gain a better understanding of the fundamental physics. The problem it was reduced to a 2D axisymmetric problem, thus omitting certain observed physics such as the highly three dimensional problem of water curtain breakup. The governing equations for this problem are then reduced from the general Navier-Stokes to the following (2D axisymmetric, laminar and incompressible):

$$\rho_i \left(\frac{\partial u_r}{\partial t} + u_r \frac{\partial u_r}{\partial r} + u_z \frac{\partial u_r}{\partial z} \right) = -\frac{\partial p}{\partial r} + \mu \left[\frac{1}{r} \frac{\partial}{\partial r} \left(r \frac{\partial u_r}{\partial r} \right) + \frac{\partial^2 u_r}{\partial z^2} - \frac{u_r}{r^2} \right] + S_{i,s} \quad (2.3)$$

$$\rho_i \left(\frac{\partial u_z}{\partial t} + u_r \frac{\partial u_z}{\partial r} + u_z \frac{\partial u_z}{\partial z} \right) = -\frac{\partial p}{\partial z} + \mu \left[\frac{1}{r} \frac{\partial}{\partial r} \left(r \frac{\partial u_z}{\partial r} \right) + \frac{\partial^2 u_z}{\partial z^2} \right] + \rho g_z + S_{i,s} \quad (2.4)$$

$$\frac{1}{r} \frac{\partial}{\partial r} (r u_r) + \frac{\partial u_z}{\partial z} = 0 \quad (2.5)$$

$$S_{i,s} = \frac{\sigma \rho \kappa n_i \Gamma}{\frac{1}{2}(\rho_i + \rho_j)} \quad (2.6)$$

Where the different indices \mathbf{i} denotes the different phase ($i \neq j$). κ is the surface curvature, \mathbf{n} is the normal of the surface for phase i , and Γ is an interface indicator function, these terms makes the surface tension $S_{i,s}$. The tangential velocity is assumed to be 0 ($\mathbf{u}_\phi = \mathbf{0}$).

2.2.1 Non-Dimensional Analysis

By non-dimensionalizing the equations for this system the important dimensionless parameters for the system will appear. It is clear that this system depends on **Reynolds number**, **Froude number** and the **Weber number**, defined as following:

$$Re = \frac{UL}{\nu} \quad Fr = \sqrt{\frac{U^2}{gL}} \quad We = \frac{\rho U^2 L}{\sigma}$$

The Reynolds number for a falling film is defined by the following expression [20].

$$Re = \frac{4\delta\langle v_z \rangle \rho}{\mu} = \frac{4\Gamma}{\mu} \quad (2.7)$$

Where Γ equals the flow rate per unit width of the film [21]. Experimental observations for falling films shows that there are three different flow regimes [20].

Laminar flow with negligible rippling	$Re < 20$
Laminar flow with pronounced rippling	$20 < Re < 1500$
Turbulent flow	$Re > 1500$

The Froude number can be interpreted as the ratio between inertia and gravity. This parameter is very important when it comes to channel flows as open channel flows are freely deformable and not drive by a pressure gradient. Similar to the Reynolds number, there exists different flow regimes, the regimes are [22] :

Subcritical flow	$Fr < 1.0$
Critical flow	$Fr=1$
Supercritical flow	$Fr > 1$

The Froude number is a measurement on how fast information travels. A subcritical flow would enable downstream flow to affect the upstream flow, in a supercritical regime this is not possible. An example of this is to introduce a disturbance in the flow such as a stick. Depending on the Froude regime waves will form either upstream, at the stick or after the stick. If waves are able to form upstream of the stick, the flow is in the subcritical regime.

The Weber number can be thought of as a measure of the relative importance of the fluid's inertia compared to its surface tension. In free falling films of water, there has been found that a Weber of unity or more is needed to stabilize the sheet behaviour. If we have $We \leq 1$, transient holes and complete breakup of the thin sheet of water have been observed [23]. However, the surface tension need not be included in the model when $We \geq 1$ [24].

2.3 Analytical Solution

The problem at hand can be split into two parts, namely the flow of the liquid down the inclined plate and the free-falling film. For the flow of water on the inclined plane, available analytical solutions can be utilized [20]. It is worth noting however, that these solutions are developed for the laminar region, incompressible flow, constant viscosity and also non-concentric inclined planes and should therefore not be used as anything else than an estimate. The edge effect and disturbances are also neglected in order to produce the following expressions. In short, these are not to be used as anything other than an estimate.

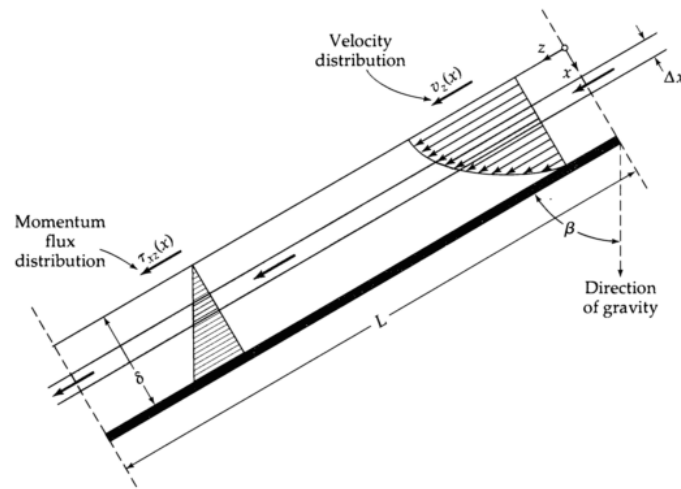


Figure 2.2: Momentum flux distribution and velocity distribution along with the Δx shell. Figure from [20].

A momentum shell balance for the z-momentum taken along the length of the inclined plane with a shell thickness of Δx yields the following expressions for the maximum and average velocity along the plane:

$$v_{z,max} = \frac{\rho g \delta^2 \cos \beta}{2\mu} \quad (2.8)$$

$$\langle v_z \rangle = \frac{\rho g \delta^2 \cos \beta}{3\mu} = \frac{2}{3} v_{z,max} \quad (2.9)$$

The film thickness δ can be given in either terms of average velocity or in terms of massflow:

$$\delta = \sqrt{\frac{3\mu \langle v_z \rangle}{\rho g \cos \beta}} = \sqrt[3]{\frac{3\mu \dot{m}}{\rho^2 g W \cos \beta}} \quad (2.10)$$

For further details about the derivation, the reader is referred to [20].

2.4 Modelling

2.4.1 Turbulence

Turbulence can be encountered every single day in different applications ranging from heat exchangers to cigarette smoke. Turbulent flows are often used in chemical reactors, heat exchangers etc because of the increased heat- and mass-transfer rates. Turbulence is something most of us might have a intuitive understanding of, but in order to model it we need to have a definition we can work with. It is important to understand that turbulence is a characteristic of the flow and not the fluid, i.e. all fluids can behave turbulently. Turbulence is characterised by chaotic motion and irregular motion, according to Hinze [25] the following characterizes turbulence:

Turbulent fluid motion is an irregular condition of flow in which the various quantities show random variation with time and space coordinates, so that statistically distinct average values can be discerned.

One could solve these irregularities simply by doing a direct numerical simulation (DNS), but this approach is extremely computationally expensive and is mostly used for research for small domains at moderate Reynolds numbers. For engineering purposes, the turbulence is not solved for directly but rather modelled. The first step of modelling turbulence is decomposing the flow variables in one averaged part and one fluctuating part, a mathematical method referred to as Reynolds decomposition demonstrated below.

$$U_i = \langle u_i \rangle + u_i \quad (2.11)$$

$$p = \langle p \rangle + p \quad (2.12)$$

The decomposed quantities in equations 2.11 and 2.12 are then substituted in to the Navier-Stokes equations, yielding the Reynolds Averaged Navier Stokes equations (RANS). This operation then introduces an unknown to the system, namely the Reynolds Stress tensor.

$$\tau_{ij} = -\rho \langle u_i u_j \rangle \quad (2.13)$$

This is known as a closure problem, and to solve it a often used framework is relating the stress terms to the mean flow quantities. Relating these terms are done using the Boussinesq approximation which reads:

$$\frac{\tau_{ij}}{\rho} = -\langle u_i u_j \rangle = \nu_T S_{ij} - \frac{2}{3} k \delta_{ij} \quad (2.14)$$

$$S_{ij} = \frac{1}{2} \left(\frac{\partial \langle U_i \rangle}{\partial x_j} + \frac{\partial \langle U_j \rangle}{\partial x_i} \right) \quad (2.15)$$

Where S_{ij} is the strain-rate tensor and k the turbulent kinetic energy per unit mass. The turbulent kinetic energy is defined as half the trace of the Reynolds stress tensor 2.13, $k = \frac{1}{2} \langle u_i u_i \rangle$ [24]. By utilizing equation 2.14, the transport of momentum is treated as a diffusive process, analogous to molecular diffusion, using the turbulent

viscosity. Turbulence models based on the Boussinesq approximation are most often referred to as eddy viscosity models.

Given that turbulence is a diffusive process, energy is needed to sustain it. The energy that sustains the turbulent eddies are extracted from the mean flow. Since energy can not disappear it is then transferred to smaller and smaller scales in what is known as the energy cascade. At the smallest scales of turbulence, the energy is then dissipated as heat due to viscous stress by molecular viscosity [24].

2.4.2 k - kl - ω - Turbulence Model

The k-kl- ω turbulence model [4,6] was chosen for this problem due to its transition sensitivity and hands off set up. A transition sensitive turbulence is needed in favour for the standard k- ω -model because of the turbulence filter, which effectively dissipates the turbulent kinetic energy before the ledge.

$$\frac{\partial k}{\partial t} + \langle U_j \rangle \frac{\partial k}{\partial x_j} = \nu_T \left[\left(\frac{\partial \langle U_i \rangle}{\partial x_j} + \frac{\partial \langle U_j \rangle}{\partial x_i} \right) \frac{\partial \langle U_i \rangle}{\partial x_j} \right] - \beta k \omega + \frac{\partial}{\partial x_j} \left[\left(\nu + \frac{\nu_T}{\sigma_k} \right) \frac{\partial k}{\partial x_j} \right] \quad (2.16)$$

$$\nu_T = \frac{k}{\omega} \quad (2.17)$$

The first term on the right hand side of equation 2.16 is the turbulence production term, which depends on the turbulence viscosity (equation 2.17). The turbulence filter effectively sets k equal 0 in the turbulence filter, rendering the k- ω -model useless for the problem at hand.

Given the novelty of this project, the k-kl- ω turbulence model was chosen in favour of the correlation based model implemented in Fluent [26]. The k-kl- ω model shows promising results in various situations like cylinder in cross flow and transitional flows on flat plates [6, 27, 28]. The authors of the model also made a point out of making it a "hands-off" model [28], meaning that no fine-tuning should be needed before utilizing the model, just like the current k- ϵ models.

The k-kl- ω turbulence model [4, 6] is an eddy viscosity turbulence model based on the k - ω -model [29]. It is one of few commercially available phenomenological (*physics-based*) transitional turbulence models today [4,6]. The transition sensitivity is achieved by adding a second kinetic energy equation for the laminar kinetic energy as proposed by Mayle and Schulz [30]. The transport equations for the model are presented below.

$$\frac{Dk_T}{Dt} = P_{K_T} + R_{BP} + R_{NAT} - \omega k_T - D_T + \frac{\partial}{\partial x_j} \left[\left(\nu + \frac{\alpha_T}{\alpha_k} \right) \frac{\partial k_T}{\partial x_j} \right] \quad (2.18)$$

$$\frac{Dk_L}{Dt} = P_{K_L} - R_{BP} - R_{NAT} - D_L + \frac{\partial}{\partial x_j} \left[\nu \frac{\partial k_L}{\partial x_j} \right] \quad (2.19)$$

$$\begin{aligned} \frac{D\omega}{Dt} = & C_{\omega 1} \frac{\omega}{k_T} P_{k_T} + \left(\frac{C_{\omega R}}{f_W} - 1 \right) \frac{\omega}{k_T} (R_{BP} + R_{NAT}) - C_{\omega 2} \omega^2 \\ & + C_{\omega 3} f_\omega \alpha_T f_W^2 \frac{\sqrt{k_T}}{d^3} + \frac{\partial}{\partial x_j} \left[\left(\nu + \frac{\alpha_T}{\alpha_\omega} \right) \frac{\partial \omega}{\partial x_j} \right] \end{aligned} \quad (2.20)$$

As transition happens in two pathways, namely natural transition and bypass transition, both have their respective production term in the model. The production terms in the model are defined as following:

$$P_{k_T} = \nu_{T,s} S^2 \quad (2.21)$$

$$P_{k_L} = \nu_{T,l} S^2 \quad (2.22)$$

Where indices s and l refers to small and large scale turbulence length scale, S is the mean strain and ν is the effective eddy viscosity at the given turbulence length scale. Transition is modelled with transfer of energy from k_L to k_T , which explains why the terms R_{BP} and R_{NAT} have opposite signs in the equations for k_L and k_T . The mechanism terms R_{BP} and R_{NAT} are defined as following:

$$R_{BP} = C_R \beta_{BP} k_L \omega / f_W \quad (2.23)$$

$$R_{NAT} = C_{R,NAT} \beta_{NAT} k_L \Omega \quad (2.24)$$

R_{BP} represents the effects of the breakdown of the stream wise velocity fluctuations know as the Klebanoff modes. R_{NAT} represents the turbulence created by breakdown of the flows inherent instabilities, the breakdown of the T-S waves. To fully resolve the boundary layer, a y^+ value of below 1 is needed ($y^+ \leq 1$), as mentioned in ref [6]. The model has 20 parameters [6] that can be fine-tuned by the user, but this is beyond the scope of this thesis and thus will not be altered. For further details about the model, the reader is referred to Walters [6].

2.4.3 Volume of Fluid

Volume of fluid is a multiphase model in the Euler-Euler framework based on the work of Hirt and Nichols [31], meaning that both phases are using an Eulerian framework [24]. Volume of fluid is only an advection scheme, meaning that the momentum equations has to be solved separately along with the volume fraction in order to successfully track the interface between two or more phases. The cells of the grid are then marked with the volume fraction, where a value of unity implies a cell completely filled with phase i . The physical properties are based on the volume fraction of each cell, meaning only one set of momentum equations is needed. For the interface tracking, the compressive scheme [32] was chosen for its stability and speed [26], which is analogous to a higher order donor-acceptor scheme leading to less smearing at the interface [32, 33]. For the transient simulation an implicit formulation is used, which means that both momentum equations and volume fractions are solved iteratively together each time step. The continuity equation for the volume fraction is

$$\frac{\partial \alpha_k \rho_k}{\partial t} + \frac{\partial \alpha_k \rho_k U_{i,k}}{\partial x_i} = - \sum_{l=1}^p (\dot{m}_{kl} - \dot{m}_{lk}) \quad (2.25)$$

Volume of fluid simulations needs a high resolution mesh to fully resolve the interface between the two phases. This problem is either solved by having an extremely dense mesh from the beginning, or one can use dynamic grid adaptation. Dynamic gradient adaptation was used in this thesis.

2.5 Fluttering

It has been seen that annular fountains and their water sheets exhibits wavelike fluttering at frequencies between 2.5 to 25 Hz [34]. Although the results from Casperson [1] are based on what he refers to as "external geometries", it is mentioned that the physics should be the same. An approximate analytic solution for the flutter frequency was presented by Casperson [1]:

$$f = \frac{m + 1/4}{(v_0/g) [(1 + 2gy_0/v_0^2)^{1/2} - 1]} \quad (2.26)$$

v_0 is the downward velocity component as it enters free fall, g is the gravitational constant, y_0 is the height of the fall and m is an integer indicating the integer for the mode.

3

Experimental Set-up and Methods

The following chapter contains the experimental methods and the experimental set-up used in this thesis. The results from the experiments will be quantitatively and qualitatively compared to those obtained in Fluent. Water trajectory, velocities on the ledge, film thickness and turbulence will be compared as these quantities are important to how the fountain operates, its stability and also the aesthetics of it.

3.1 Geometry

Both the experiments and the simulations were carried out on the baseline design with added baffle, turbulence filter and smoothed ledge. To stabilize the flow before the inclined ledge, an extra wall and an aquarium filter (functions as a turbulence dampener) was added. The design has been supplied by Osar Aschan. This design is the second generation in the process, and its design is based on "hands on" experience of engineers Lasse Urholm and Lennart Norberg, as well as theoretical input from Bengt Andersson and Ronnie Andersson.

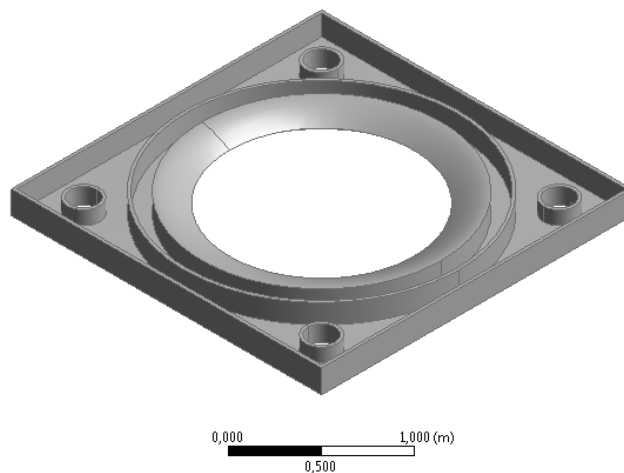


Figure 3.1: Baseline design for the fountain.

The four circular inlets are located at each corner in Figure 3.1. This design with the extra reservoir before the inclined ledge is thought to facilitate the water feed as well as keeping the fluctuation of the water surface at a minimum.

3. Experimental Set-up and Methods

An extra wall was added in the center of the circular channel, and an aquarium filter 4cm by 6cm was then added between this extra wall and the inclined ledge. These measures to dampen the turbulence were made to stabilize the flow further.



(a) Aquarium filter.



(b) Magnification of the filter.

Figure 3.2: A piece of the aquarium filter used for damping out turbulence at the inlet.

The aquarium filter and the details of it can be seen in Figure 3.2, the pores had a characteristic width of 0.5 mm and the porosity of the filter was estimated to α equal to 0.5.

The wall added in the circular water reservoir is referred to as a baffle. In this case it is effectively lowering the wall distance and thus increases the wall damping of the velocity fluctuations. The characteristic length of an annulus used in the calculations of the Reynolds number is [35]

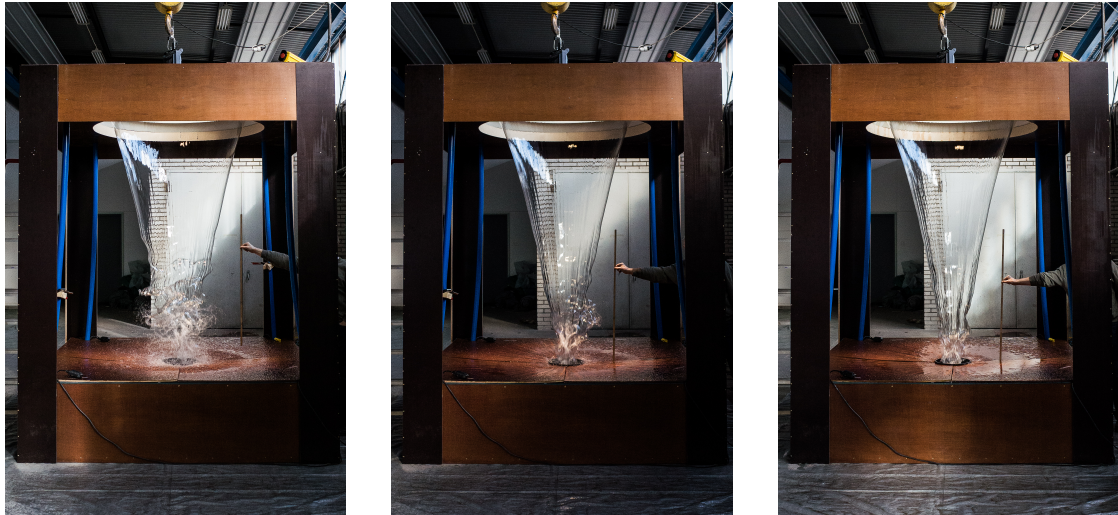
$$L = D_o - D_i$$

L is also referred to as the hydraulic diameter. By the addition of the baffle, the hydraulic diameter is effectively halved compared to the water reservoir without the baffle. This leads to a 50% reduction of the Reynolds number for the reservoir.

3.2 Experiments

3.2.1 Trajectory and Fluttering

The water is pumped from ground level to 3m using four waste water pumps (Minex). To control the mass flow of water, each individual pump has to be shut down seeing that there is no power adjustment settings. The data sheets for the pumps states that they at the given height of the model should produce a mass flow of 9 l/s each. Pictures were taken at each mass flow rate and later analysed using the software Tracker. Film clips of the same set-up were also filmed and analysed to measure the fluttering frequency. The data gathered from the experiments were then plotted using Matlab. The fountain was tested at four different flow rates; $\dot{m}=18\text{kg/s}$, $\dot{m}=27\text{kg/s}$ and $\dot{m}=36\text{kg/s}$, which equals 2,3 and 4 pumps respectively. Demonstrated below in Figure 3.3, is the difference in stability at different flow rates.



(a) 2 pumps in action.

(b) 3 pumps in action.

(c) 4 pumps in action.

Figure 3.3: The prototype of the fountain operating at different flowrates.

3.2.2 Turbulence

A flat tip syringe was used together with a 1ml pump to inject red dye at various locations in the film. At the beginning of the ledge, a self-built device to keep the tip at 5mm from the surface was used, the device is shown in Figure 3.4. Due to the curvature and thickness of the film, free-hand injections was preferred although it will introduce possibility for errors. Only the highest flow rate ($\dot{m}=36 \text{ kg/s}$) was used for these measurements.

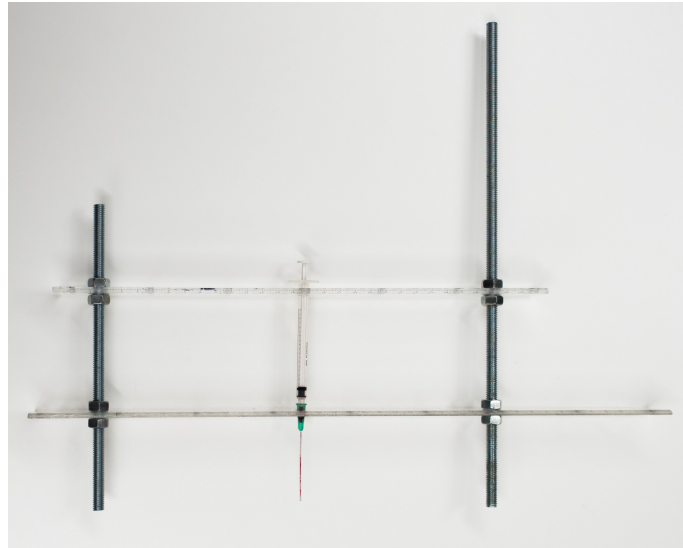


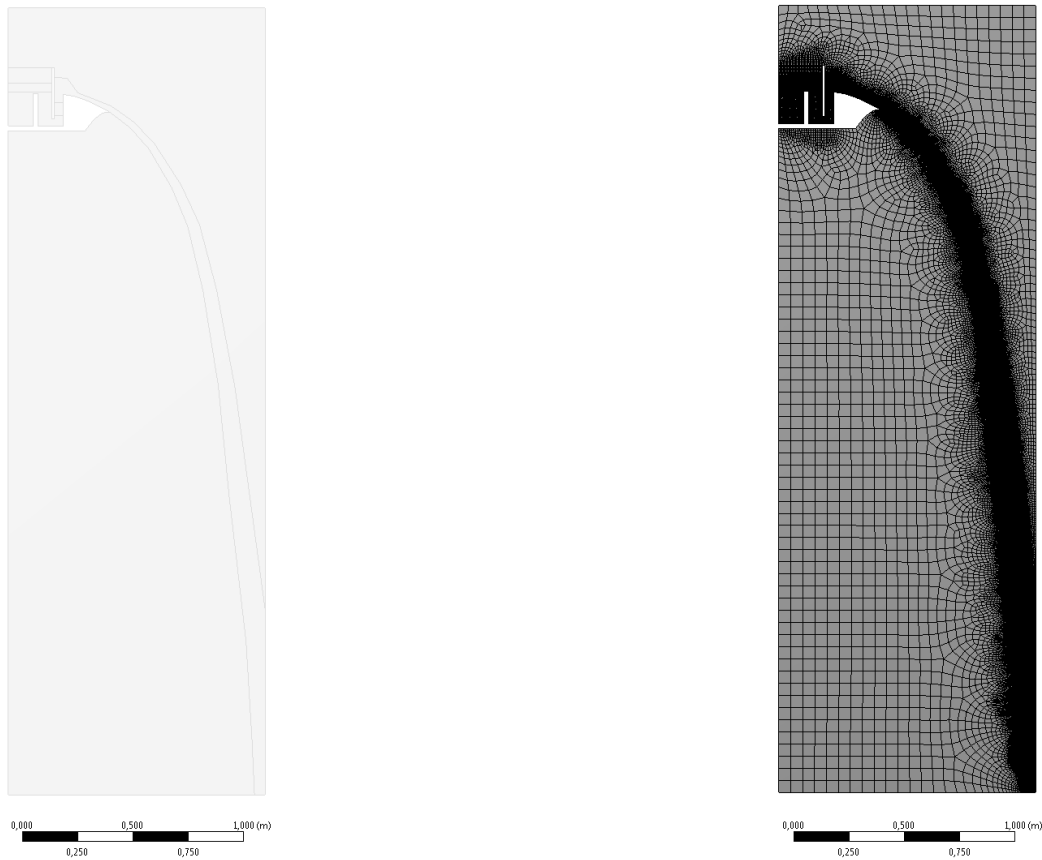
Figure 3.4: Device used to keep the tip of the syringe at desired position in the film.

3.3 Simulations

A short overview over the methods used in the calculations will be given in the following section.

3.3.1 Mesh

Three different geometries were used to create three different initial meshes. One geometry for the full-scale waterfall, two for studying the effect of the edge effect on the production of turbulence. The 3D CAD of the fountain was imported into ANSYS Design Modeler and used as a tool to make a cut-out of a 2D plane of appropriate dimensions. The meshing process consisted of manually separating the 2D geometries to enable individual face sizing in ANSYS Meshing to optimize the initial mesh, a smaller face size was set where the water film was expected to be. Figure 3.5 shows the geometry and initial mesh for the full-scale trajectory simulations. As mentioned earlier, the mesh will be dynamically refined. The initial mesh consisted of 100.778 cells, with an average orthogonal quality at 0.9786.



(a) Geometry with separated regions.

(b) Mesh.

Figure 3.5: Geometry and mesh for the trajectory calculations.

Two geometries were made to compare the effect of the edge design on the turbulence production. The mesh for comparing the different edges from the water reservoir to the ledge was refined in areas of interest.

The sharp edge mesh had an initial size of 14.457 cells, with an average orthogonal quality of 0.956. The smooth edge mesh had an initial size of 14.329 cells, with an average orthogonal quality of 0.982.

3.3.1.1 Adapting Mesh

In order to correctly capture the interface between the two phases, a relatively fine mesh is needed. In free surface problems like this, the mesh needs to be dynamically refined to obtain the sharpest interface possible at the lowest computational costs.

$$|e_i| = \langle A_{cell} \rangle^{\frac{r}{2}} |\nabla f| \quad (3.1)$$

Where e_i is the error indicator, A_{cell} is the cell area, r is the gradient volume weight, and ∇f is the Euclidean norm of the gradient of the desired field variable, f , in this case the water fraction. Fluent was set to refine the mesh in cells that had



(a) Sharp edge.

(b) Smooth edge.

Figure 3.6: Sharp and smooth edge design for studying edge effects on turbulence production.

a normalized gradient of 0.1, coarsen at values below 0.1. Due to problems with the automatic refinement and to assure a sharp interface, the mesh was also refined manually with both gradient adaptation and iso-value for water fraction (from 0.2 to 0.95).

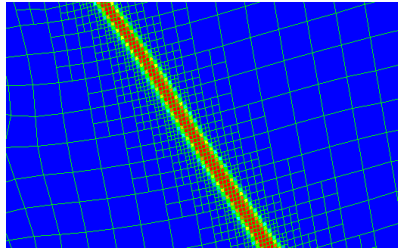


Figure 3.7: Dynamically adapted mesh.

3.3.2 Pressure Drop

To correctly model the behaviour of the flow through the filter, a correct set of resistance parameters is needed. The porous zone is modelled as an added momentum sink in the momentum equations. When the flow through the porous zone is laminar, the pressure drop can be considered to be proportional to the velocity as described by Darcy's law:

$$\nabla P = -\frac{\mu}{\alpha} \mathbf{v} \quad (3.2)$$

Where α is the permeability of the porous zone and μ is the viscosity of the fluid, the porosity for the porous zone was set to 0.5.

3.3.3 Numerical methods

The simulations were all done with a transient solution, the reason being that this flow is inherently dynamic. The time step size is calculated by using the CFL criteria (Courant-Friedrich Lewy), stated as

$$\Delta t < CFL \cdot \min\left(\frac{\rho(\Delta x)^2}{\Gamma}, \frac{\Delta x}{U}\right) \quad (3.3)$$

Where $CFL=5$ in this case, as a fully implicit solver is being used [24].

Furthermore, the Pressure-Implicit with Splitting of Operators (PISO) is used in for these simulations along with Body force weighted scheme for the pressure seeing that there are large body forces. Rough estimates of the Weber number at different locations of the film was found to be higher than unity, thus enabling us to omit surface tension modelling in the calculations.

As previously stated the main focus of this thesis is to make an axisymmetric model of the fountain, this simplification of the model will have an impact on the results. The prototypes of the fountains both have inlets that by nature are three dimensional. The prototype utilizes perforated plastic tube system for the water inlet. Unlike the inlets seen in the prototypes, the simulations are carried out with an uniform distribution of water. The flow rates are set using experimental data and data sheets for the pumps.

The solution was initialized using the standard initialization with very low values for the turbulence. The following settings were used to minimize the initial turbulence in the system, turbulent kinetic energy $1e-6m^2/s^2$, laminar kinetic energy $1e-6m^2/s^2$ and specific dissipation rate $10s^{-1}$. The initial conditions are of great importance as they affect stability of the solution as well as simulation time.

To judge the convergence of the simulation, a control surface (line) was added across the free-falling water film at various positions to ensure that $\dot{m}_{in} - \dot{m}_{out} = 0$, i.e. mass balance was reached. Calculations show that the smaller meshes need more than 10s to reach steady state.

To measure the velocity in the film at the ledge before entering free-fall, a mass-weighted average over a facet that covers the film is calculated. The mass-weighted average is calculated using the following expressions:

$$\frac{\int \phi \rho |\vec{v} \cdot d\vec{A}|}{\int \rho |\vec{v} \cdot d\vec{A}|} \quad (3.4)$$

4

Results and Discussions

In this chapter the results from the experiments will be compared with those results obtained from simulations. The results will be discussed continuously.

4.1 Full Scale Experiments and Simulations

4.1.1 Trajectory

The trajectory of the falling film was examined, experiments done at four different flow rates yields the following results. The lowest flow rate did not result in a continuous film, and is not plotted. Results from calculations are plotted together with experimental data.

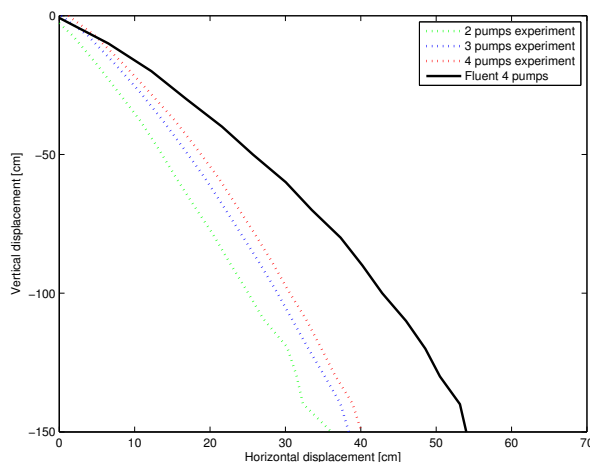


Figure 4.1: X-Y coordinates for the trajectory of the falling film, given in centimetres from the ledge. Zero level for y-coordinates denotes 10cm below ledge.

As expected, higher flow rates leads to higher radial velocity. The measurements starts 10 cm below ledge, as it was the highest point that could be observed from the camera's point of view. As can be seen in Figure 4.1, the initial radial velocity component is greater in the results from the simulations than in the experiments. It is possible that the boundary conditions for the water feed in the simulations is slightly higher than reality in the experiments, leading to a thicker film and thus a higher momentum. It is important to realize that the experiments were carried out on the full scale prototype.

4.1.2 Fluttering

During the trajectory measurements, the fluttering frequency was also investigated. The camera used limited the temporal resolution to 60 frames per second, which proved to be too coarse to precisely determine the frequency. The longitudinal waves on the free falling film on water display a higher frequency than can be correctly determined by the video analysis and is thus inconclusive. This analysis only shows that the flutter frequency is higher than 30 Hz.

4.2 Turbulence

Video analysis shows signs of intermittent turbulent spots on the ledge. Figure 4.2 shows characteristics of a mostly laminar flow starting at the top of the inclined ledge. Intermittent turbulent behaviour can be observed starting from 8-16 cm from the end of the ledge (marked with a red arrow). Notice that the dye shows coexistence of laminar and turbulent spots at the same time (marked in black ellipsis). The first turbulent spot in Figure 4.2 starts at 12 cm - 9 cm (red arrow). Video analysis shows that $\gamma(10\text{cm}) = 0.522$, which means that the flow is turbulent 52.2% of the time. As mentioned earlier, injecting the dye at the exact depths proved difficult. The tip of the syringe was flat and perpendicular to the stream, this might have lead to higher turbulence at the injection point. Several injections at different depths and administered with a syringe parallel to the flow of the film would have been preferred. The best way to measure would be using non-intrusive measurement tools such as Laser Doppler velocimetry.

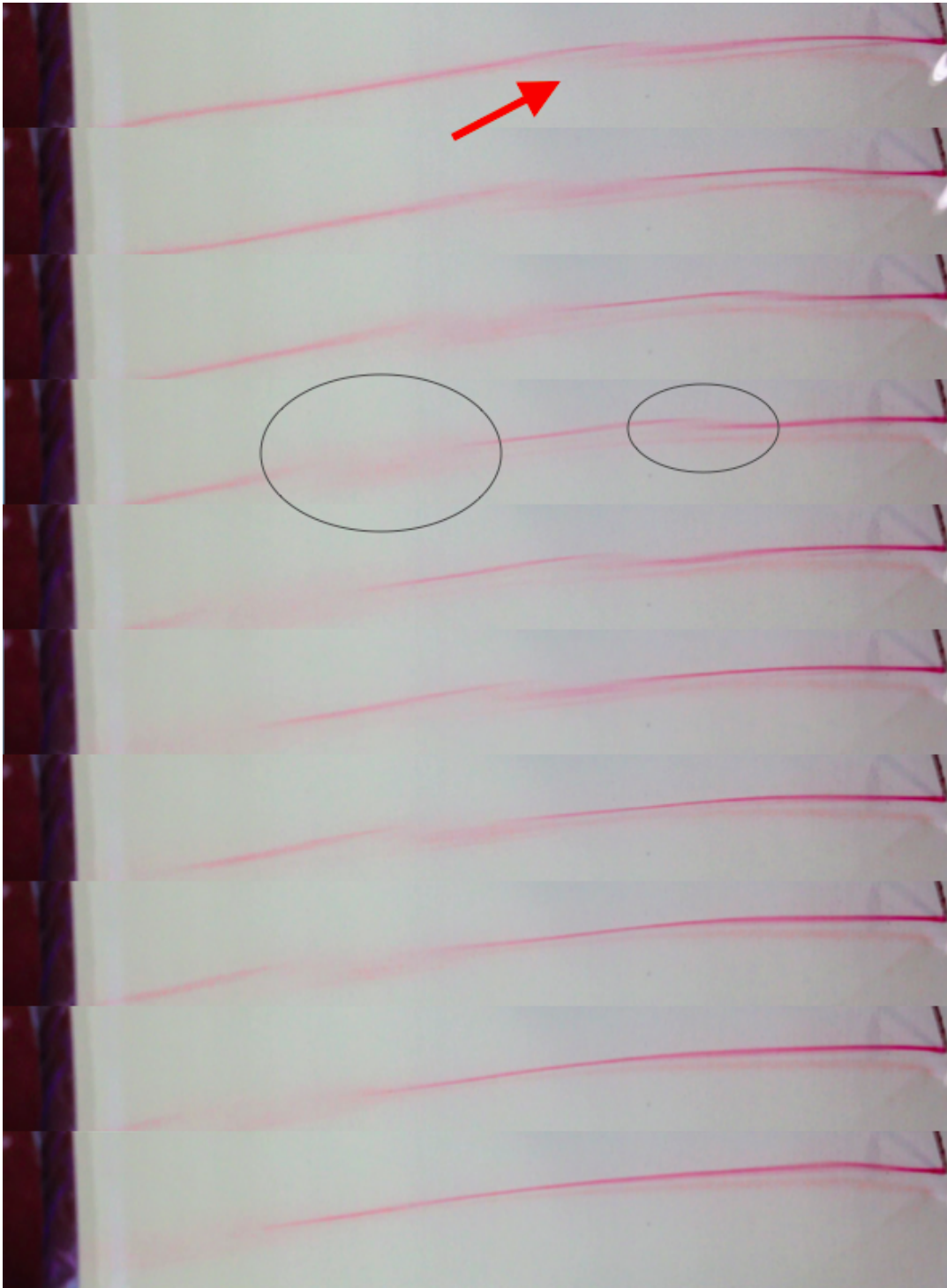


Figure 4.2: Dye injections 13cm from the ledge end, taken at an interval of $1/30$ s. Best viewed in colour.

4.3 Velocities at Ledge

The simulations were carried out on the baseline design with smoothed edge, added baffle and turbulence filter. The original design was tested at three different flow rates corresponding to 2,3 and 4 pumps respectively. The different designs were compared at the maximum flow rate at \dot{m} equals 36 l/s. Average velocities, velocity components and film thickness were measured.

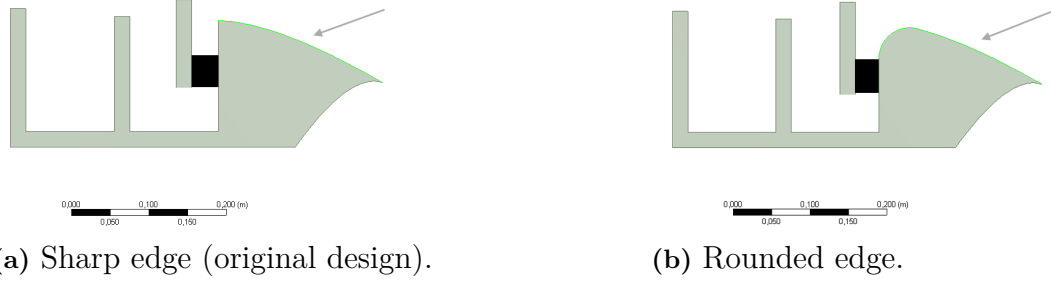


Figure 4.3: Location for the data extraction is marked with a grey arrow. The black rectangle illustrates the turbulence filter.

Table 4.1: Data for the sharp edge (original design), at different flow rates.

Flowrate	$\langle V \rangle$ [m/s]	$\langle V_z \rangle$ [m/s]	$\langle V_r \rangle$ [m/s]	δ [mm]	Re
36 l/s	1.252	0.611	1.093	6.6160	33007
27 l/s	1.233	0.602	1.077	5.0900	25009
18 l/s	1.198	0.582	1.047	3.5574	16982

Table 4.2: Data for the two designs.

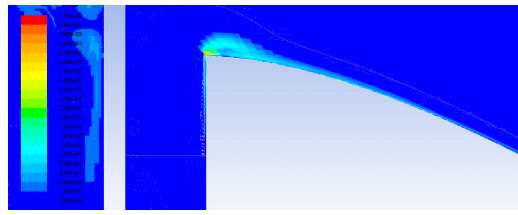
Design	$\langle V \rangle$ [m/s]	$\langle V_z \rangle$ [m/s]	$\langle V_r \rangle$ [m/s]	δ [mm]	Re
Sharp edge	1.252	0.611	1.093	6.6160	33007
Smooth edge	1.240	0.606	1.081	7.1906	35530

Table 4.1 indicates a relatively small change in average velocity when increasing the flow rate. Furthermore, the Reynolds numbers for at the different flow rates are all in the turbulent regime. When comparing the data for the 27 l/s case and the 36l/s case in table 4.1 with experimental data from Figure 4.1, it is reasonable to believe a thick water film is needed. A more stable free-falling film with a thicker water film is consistent with the results from Caspersson [1, 34, 36] to some extent.

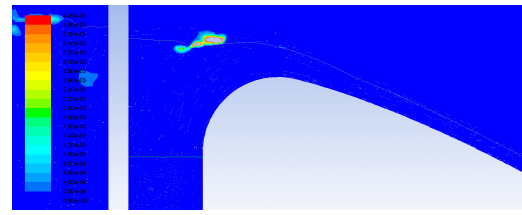
Table 4.2 shows that the water film thickness on the inclined plane is noticeably thicker with the smooth edge design. Comparing the velocities, it is apparent that the velocity is slightly reduced with the smooth edge design.

4.4 Edge effects

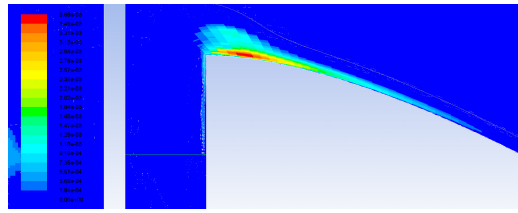
Data extracted from the inclined ledges seen in Figure 4.3, air/water interface as well as turbulence filter is marked with grey lines. Presented in Figure 4.4 are comparisons of the different turbulent quantities at the ledge. The water/air interface is marked with a grey line and all the quantities are scaled with respect to the maximum values obtained for the sharp edge. Figure 4.4 shows that the sharp edge has significantly higher production and values for both laminar kinetic energy as well as turbulent kinetic energy. The absolute values for the turbulent quantities should not be used, but rather the results should be compared. It is quite obvious that the sharp edge produces several times higher values of all the turbulent quantities than that of the smoothed edge. The reason for this difference in turbulence levels for the two different designs are the flow separation that occurs at ledge, as shown in Figure 4.5. It is observed that the water level before the the inclined ledge is higher for the sharp edge design than for the rounded edge due to the flow separation. The turbulence seen in the contour plots for the smooth edge is limited to a small area in the water/air interface and should be ignored.



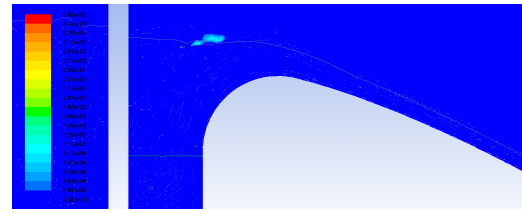
(a) Sharp edge, contour with laminar K



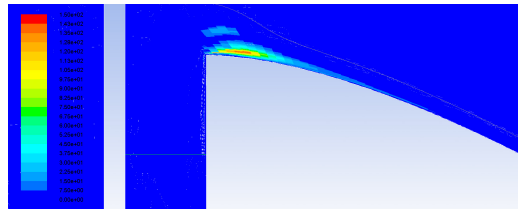
(b) Smooth edge laminar K



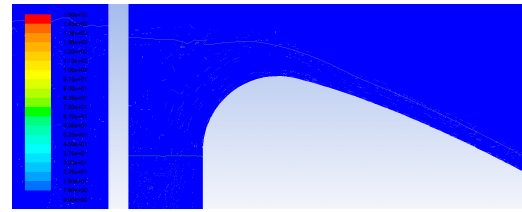
(c) Sharp edge contour of turbulent K



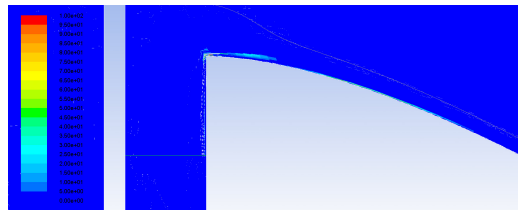
(d) Smooth edge, contour of turbulent K



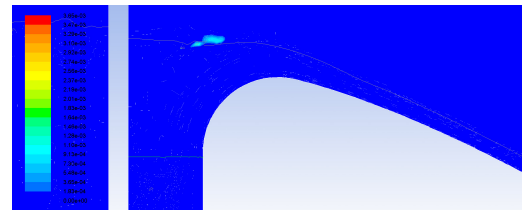
(e) Sharp edge, production of turbulent K



(f) Smooth edge, contour of turbulent K

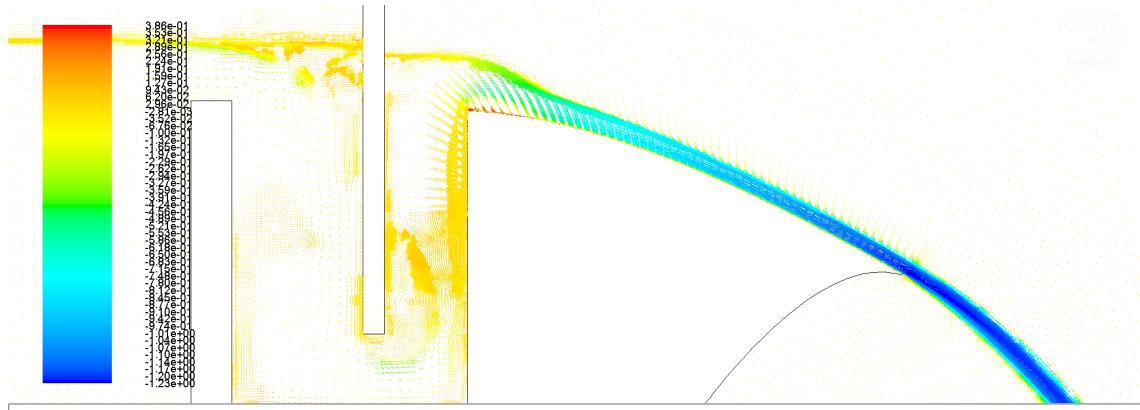


(g) Sharp edge, production of tlaminar K

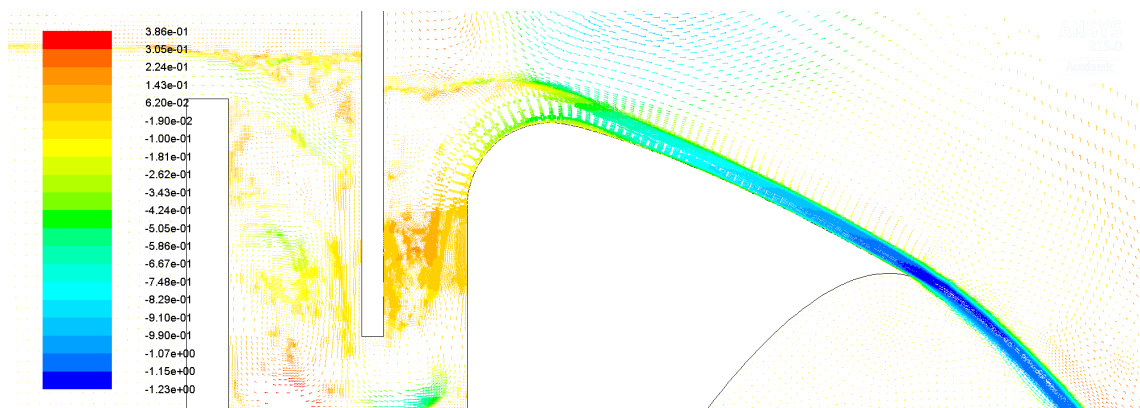


(h) Smooth edge, contour of laminar K

Figure 4.4: Comparison of different turbulent quantities for the two designs. Note that all quantities are scaled after the unmodified edge. The water level is marked with a black line. Best viewed in colour.



(a) Velocity vectors coloured by radial velocity for the sharp edge.



(b) Velocity vectors coloured by radial velocity for the smooth edge.

Figure 4.5: Velocity vectors coloured by radial velocity for the different designs.

Figure 4.5 shows the velocity vectors coloured by the radial velocity. When comparing the two different designs, it is apparent that the flow separates due to the sharp edge. This separation leads to swirling flow which will sustain turbulence on the edge via the turbulence cascade. This behaviour is not displayed for the smooth edge

4.5 Discussion

As presented in chapter 2 theory, there has been observed fluttering of free-falling films from similar types of set-up as seen in this thesis. Video analysis (frame by frame) of the fountain shows that it exhibits a fluttering as described by Casperson [1, 34, 36–38]. However, the analysis is inconclusive as the fluttering exceeds the temporal resolution of the camera utilized (60 frames per second), thus suggesting the fluttering exceeds the frequency mentioned by Casperson [1, 34, 36–38].

As mentioned before, this problem is highly complex and really underlines the "problem" with computational fluid dynamics. Computational fluid dynamics is a very powerful tool, but there needs to be a good/better theoretical understanding of the flow before even attempting solving this with CFD. In hindsight, more focus should be put on minimizing the turbulence in the water reservoir. The pore size of the filter, the filter's permeability, shape of the water reservoir and also materials used could be investigated further. The inlet is believed to have a substantial impact on the film stability. The current set-up uses four waste water pumps each with outlets in the four corners of the prototype. The outlets of the pumps are then connected to a perforated plastic tube system connected with T-junctions at every corner. Based on the force exerted from the water on the fountain at each T-junction, some speculations has been made that this disturbance might affect the stability of the falling water film. However, it is noted that the final version of the fountain will be made with more rigid materials that most likely will mitigate these problems.

It proved difficult to get scientifically proven, quantifiable results on the resulting geometry. This problem is not trivial, and proves how difficult it can be implementing CFD in development processes. The length scale difference between the fountain and the free falling film is enormous, making it hard to correctly predict using student licenses (max 500.000 cells). Even without the cell number limitation, this problems needs a lot of computational power to give accurate results since the problem is transient. CFD is a very potent tool, but one need to understand when it is beneficial and when it is not. For instance in this case it can be argued that more "hands on" experiments would likely be better than CFD.

When attacking a problem like this, a uniform quadrilateral mesh with dynamic adaptation paired with a more simplified geometry is highly recommended. In Figure 3.6, one can observe the sharp ledge before the water hits free-fall, this part is particularly difficult to mesh with acceptable quality. Altering the geometry to facilitate meshing should be done, but proved difficult with the tools available.

5

Conclusion

The $k\text{-}\kappa\text{-}\omega$ -turbulence model combined with VOF and open channel flow fails to correctly calculate the trajectory of the free falling film. Analysis of the trajectory of the free-falling water film from simulations also implies that the effect of gravity acting on the film is underestimated. Another reason for the large discrepancies between the experimental results and the results from the simulations might be due to a lower mass flow rate in the experiments. The water has to be elevated more than 2m which cause a significant pressure difference, this might lead to a lower mass flow rate than assumed. It proved difficult to correctly measure the water flow experimentally, therefore data sheets for the pumps were used instead. Mesh independence test suggests a higher flow rate was used in simulation then what was used in experiments. To verify that the problem is indeed with the inlet conditions, more effort should be made to determine the correct amount of water for the inlets. As can be seen in Figure 4.5 the original design results in a separation of the flow and a vortex can be seen when transitioning from inlet to ledge. The same behaviour is not displayed for the rounded edge. Comparing the two designs it is apparent that the smoothing of the ledge leads to a more stable water film on the ledge. When comparing the results show a drastic difference in laminar kinetic energy as well as turbulent kinetic energy. As an effect of this less pronounced transition leads to a lower acceleration of the water entering the ledge resulting in a calmer flow and lower velocity. As previously mentioned, the build-up of laminar-kinetic energy is an important factor of turbulence production. It can therefore be concluded that the smoother transition from basin to ledge decreases the laminar kinetic energy and thus the chance for the flow to develop turbulence before leaving the ledge.

It is known that surface roughness has an effect on the transition of the flow [2]. It is also shown that annular fountains are extremely prone to instabilities when the water film is not uniform [1]. From these two facts we can draw the conclusion that the fountain needs to be completely levelled, and the surface has to be as smooth as it can possibly be. Experiments show that the flow transitions from laminar to turbulent on the inclined ledge which leads to instability in the free-falling film. The baffle together with the turbulence filter proved to greatly dampen the turbulence in the water reservoir, leading to a more stable water film. Furthermore, it is concluded that there is a limit to what CFD can be used for. Although large discrepancies were found comparing the trajectories of experiments with simulations, the simulations can be used to discover trends etc. The use of CFD should be limited to examine details of the design, and has proven helpful in design guidance for further development of the fountain.

5.1 Future studies

To gain a better understanding of the physics in this fountain, it is advised to further investigate the physics in the water reservoir. The baffle, placement, dimensions and if adding more of them would affect the flow. The angle of the baffle could also be adjusted so the water channel just before the ramp would widen substantially causing a drop in Reynolds number. The effect of the turbulence filter and its dimensions could be examined further. The dimensions would then be adjusted to minimize the energy in the flow before the ramp, thus leading to a more stable fountain. The ledge design should be further investigated to find the optimal design and thus minimizing the kinetic energy at the inclined ledge. It would be interesting to test the effect of rotation on the flow ($u_\phi \neq 0$), as it would introduce an angular momentum. Angular momentum will be constant through the system, thus resulting in a higher azimuthal velocity as the water sheets contracts. This is believed to stabilize the flow by minimizing the longitudinal surface waves that are believed to be the reason for the fluttering.

Bibliography

- [1] L. W. Casperson, “Fluttering fountains: Annular geometry,” *Journal of Applied Physics*, vol. 79, no. 3, p. 1275, 1996.
- [2] M. T. Schobeiri, “Laminar-turbulent transition,” in *Fluid mechanics for engineers: a graduate textbook*, pp. 233–269, Berlin: Springer, 2010.
- [3] X. Wang and K. Walters, “Computational Analysis of Marine-Propeller Performance Using Transition-Sensitive Turbulence Modeling,” *Journal of Fluids Engineering*, vol. 134, no. 7, p. 071107, 2012.
- [4] D. K. Walters and J. H. Leylek, “A New Model for Boundary Layer Transition Using a Single-Point RANS Approach,” *Journal of Turbomachinery*, vol. 126, no. 1, p. 193, 2004.
- [5] Z. Zhang and C. Kleinstreuer, “Laminar-to-turbulent fluid-nanoparticle dynamics simulations: Model comparisons and nanoparticle-deposition applications,” *International Journal for Numerical Methods in Biomedical Engineering*, vol. 27, pp. 1930–1950, Dec. 2011.
- [6] D. K. Walters and D. Cokljat, “A Three-Equation Eddy-Viscosity Model for Reynolds-Averaged Navier–Stokes Simulations of Transitional Flow,” *Journal of Fluids Engineering*, vol. 130, no. 12, p. 121401, 2008.
- [7] T. Cebeci and J. Cousteix, *Modeling and computation of boundary-layer flows: laminar, turbulent and transitional boundary layers in incompressible flows*. Long Beach, Calif; Berlin: Horizons Pub, 2nd rev. and extend ed., 2005; 1999.
- [8] H. Schlichting, *Boundary-layer theory*. New York: McGraw-Hill, 1979.
- [9] G. Schubauer and H. Skramstad, “Laminar boundary-layer oscillations and transition on a flat plate,” *Journal Of Research of the National Bureau of Standards*, vol. 38, no. 2, pp. 251–292, 1947.
- [10] G. B. Schubauer and P. S. Klebanoff, “Contributions on the mechanics of boundary-layer transition,” *Journal of research of the National Bureau of Standards (Washington, D.C. : 1955)*, no. 1, p. 12, 1955.
- [11] D. D. Sanders, W. F. O’Brien, R. Sondergaard, M. D. Polanka, and D. C. Rabe, “Predicting Separation and Transitional Flow in Turbine Blades at Low Reynolds Numbers—Part I: Development of Prediction Methodology,” *Journal of Turbomachinery*, vol. 133, no. 3, p. 031011, 2011.

- [12] G. J. Walker, “The Role of Laminar-Turbulent Transition in Gas Turbine Engines: A Discussion,” *Journal of Turbomachinery*, vol. 115, no. 2, p. 207, 1993.
- [13] D. Arnal and G. Casalis, “Laminar-turbulent transition prediction in three-dimensional flows,” *Progress in Aerospace Sciences*, vol. 36, no. 2, pp. 173–191, 2000.
- [14] P. Schlatter, L. Brandt, H. C. de Lange, and D. S. Henningson, “On streak breakdown in bypass transition,” *Physics of Fluids*, vol. 20, no. 10, pp. 1–15, 2008.
- [15] J. Fürst, P. Straka, and J. Příhoda, “Modelling of natural and bypass transition in aerodynamics,” *EPJ Web of Conferences*, vol. 67, p. 02030, 2014.
- [16] S. J. Leib, D. W. Wundrow, and M. E. Goldstein, “Effect of free-stream turbulence and other vortical disturbances on a laminar boundary layer,” *Journal of Fluid Mechanics*, vol. 380, pp. 169–203, 1999.
- [17] P. Ricco, “The pre-transitional Klebanoff modes and other boundary-layer disturbances induced by small-wavelength free-stream vorticity,” *Journal of Fluid Mechanics*, vol. 638, p. 267, 2009.
- [18] M. E. McCormick, “An Analysis of the Formation of Turbulent Patches in the Transition Boundary Layer,” *Journal of Applied Mechanics*, vol. 35, no. 2, p. 216, 1968.
- [19] F. M. White, *Viscous fluid flow*. New York: McGraw-Hill, 1991.
- [20] R. B. Bird, W. E. Stewart, and E. N. Lightfoot, *Transport phenomena*. New York: Wiley, 2. ed., 2002.
- [21] I. Mudawar and R. Houpt, “Mass and momentum transport in smooth falling liquid films laminarized at relatively high Reynolds numbers,” *International journal of heat and mass transfer*, vol. 3, no. 14, pp. 3437–3448, 1993.
- [22] F. M. White, *Fluid mechanics*. Singapore: McGraw-Hill, 7th in si units. ed., 2011.
- [23] J. S. Roche, N. Le Grand, P. Brunet, L. Lebon, and L. Limat, “Perturbations on a liquid curtain near break-up: Wakes and free edges,” *Physics of Fluids*, vol. 18, no. 8, pp. 1–14, 2006.
- [24] B. Andersson, R. Andersson, L. Håkansson, M. Mortensen, R. Sudiyo, and B. G. M. van Wachem, *Computational Fluid Dynamics for Engineers*. Cambridge University Press, Cambridge, 2011.
- [25] J. O. Hinze, *Turbulence*. New York: McGraw-Hill, 2. ed., 1975.
- [26] ANSYS® Academic Research, Release 15.0, Help System, *ANSYS Fluent Theory Guide*. ANSYS, Inc.

-
- [27] D. S. Holloway, D. K. Walters, and J. H. Leylek, "Prediction of unsteady, separated boundary layer over a blunt body for laminar, turbulent, and transitional flow," *International Journal for Numerical Methods in Fluids*, vol. 45, no. 12, pp. 1291–1315, 2004.
- [28] D. K. Walters and J. H. Leylek, "Computational Fluid Dynamics Study of Wake-Induced Transition on a Compressor-Like Flat Plate," *Journal of Turbomachinery*, vol. 127, no. 1, p. 52, 2005.
- [29] D. C. Wilcox, *Turbulence modeling for CFD*. La Cãnada, Calif: DCW Industries, 2006.
- [30] R. E. Mayle and A. Schulz, "The path to predicting bypass transition," *Journal of Turbomachinery*, vol. 119, no. 3, p. 405, 1997.
- [31] C. Hirt and B. Nichols, "Volume of fluid (VOF) method for the dynamics of free boundaries," *Journal of Computational Physics*, vol. 39, pp. 201–225, Jan. 1981.
- [32] O. Ubbink, "Numerical prediction of two fluid systems with sharp interfaces," *Splash*, no. January 1997, p. 69, 1997.
- [33] G. H. Yeoh and J. Tu, *Computational Techniques for Multiphase Flows*. US: Butterworth Heinemann, 2010; 2009.
- [34] L. Casperson, "Fluttering Fountains," *Journal of Sound and Vibration*, vol. 162, no. 2, pp. 251–262, 1993.
- [35] R. W. Fox, A. T. McDonald, and P. J. Pritchard, *Introduction to fluid mechanics*. New York: Wiley, 6. ed., 2004.
- [36] L. W. Casperson, "Fluttering fountains: Stability criteria," *Journal of Applied Physics*, vol. 75, no. 10, pp. 4892–4894, 1994.
- [37] L. W. Casperson, "Fluttering fountains: Simplified models," *Journal of Applied Physics*, vol. 74, no. 8, p. 4894, 1993.
- [38] L. W. Casperson, "Fluttering fountains: Stability criteria," *Journal of Applied Physics*, vol. 75, no. 10, pp. 4892–4894, 1994.